High-Frequency Behavior of Laminated Iron-Core Inductors for Filtering Applications

U. Reggiani, G. Grandi, G. Sancineto
Dept. of Electrical Engineering
University of Bologna
Viale Risorgimento 2, 40136 - Bologna, Italy

M.K. Kazimierczuk
Dept. of Electrical Engineering
Wright State University
Dayton, OH 45435, USA

A. Massarini
Dept. of Engineering Sciences
University of Modena and Reggio Emilia
via Campi 213/B, Modena - 41100, Italy

Abstract - **Laminated iron-core inductors are largely used in power electronics applications. In particular, coupling reactors and filtering devices employ such a type of inductors in the medium-high power range. In this paper, a model is proposed to represent the behavior of these inductors that are used in switching converters, i.e., for excitation frequencies above several kHz.**

I. INTRODUCTION

In many power filtering devices, laminated iron-core inductors are preferred over both air-core and ferrite-core inductors. The air-core inductors are less expensive, but present higher size and copper losses. Furthermore, the leakage magnetic field is important at low frequencies. The use of ferrite as a core medium offers some advantages, such as lower copper losses compared to the air-core inductors and lower core losses compared to the laminated iron-core inductors. In addition, the low electric conductivity limits the eddy currents and allows the ferrite to properly operate at frequencies up to several MHz. On the other hand, the use of ferrite is restricted to applications requiring reduced core dimensions, such as small-signal high-frequency filters or small-inductance reactors, and the ferrite is quite expensive. Mainly for these reasons, the laminated iron-core inductors are widely employed in power filtering applications at low frequencies. In particular, the possibility of geometrical arrangement of the sheets in several different ways leads to very flexible core constructions, capable of satisfying most of the inductor requirements.

A critical point in the design of laminated iron-core inductors is the evaluation of the inductance behavior versus frequency and the additional core losses. Owing to the iron high electric conductivity and in spite of the core lamination, the effects produced by the eddy currents are significant starting from frequencies of several kHz.

In this paper, an analytical model taking into account the eddy currents in laminated iron-cores is developed through an one-dimensional electromagnetic field analysis. The proposed model considers the presence of air gaps in the magnetic circuit as in the inductor practical realization. The RLC circuit model shown in Fig. 1 is adopted to represent the frequency behavior of the whole inductor. The equivalent series parameters L_{ac} and R_{ac} are frequency-dependent components that take into account skin and proximity effects in the winding [1] and eddy currents in the laminated iron- core [2]. The parallel capacitance C models the turn-to-turn and turn-to-iron stray capacitances [3] and it is assumed to be independent of frequency.

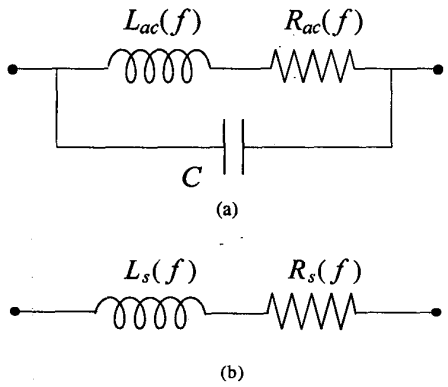

Fig. 1. Inductor models
(a) *RLC* equivalent circuit,
(b) series equivalent circuit.

II. INDUCTOR MODEL

In the following Sections, the circuit models depicted in Fig. 1 are discussed. The total inductance L_{ac}, the total ac resistance R_{ac} and the overall stray capacitance C are described and estimated in detail. For this purpose, a model for both the winding and laminated iron-cores are separately developed in Subsections *A* and *B*, respectively. In Subsection *C*, the whole inductor is considered including the parasitic capacitance, which is obtained from the inductor self-resonance measurements.

A. Winding Model

The winding resistance of an inductor increases with frequency because of the skin and proximity effects due to the time-varying electromagnetic field. The final result of these two combined effects is a reduction in the effective cross-sectional area of the wire available for the current flow. Therefore, the ac resistance R_w at high frequencies becomes

0-7803-5864-3/00/$10.00 © 2000 IEEE

greater than the dc resistance R_{wdc}. The winding ac resistance of an inductor with N_l layers can be expressed as [1]

$$R_w = R_{wdc} A \cdot \left[\frac{e^{2A} - e^{-2A} + 2\sin(2A)}{e^{2A} + e^{-2A} - 2\cos(2A)} + 2\frac{N_l^2 - 1}{3} \cdot \frac{e^{A} - e^{-A} - 2\sin A}{e^{A} + e^{-A} + 2\cos A} \right] \quad (1)$$

where A is an adimensional factor which depends on the winding geometry. The first and second term of (1) represent the skin effect and the proximity one in the winding, respectively. For a round wire with conductor diameter d the factor $A = A_r$ is given by

$$A_r = \left(\frac{\pi}{4}\right)^{\frac{3}{4}} \frac{d^{\frac{3}{2}}}{\delta_w p^{\frac{1}{2}}}, \quad (2)$$

whereas for a strip wire, having conductors with dimensions a and h (Fig.3), $A = A_s$ becomes

$$A_s = \frac{a}{\delta_w}\sqrt{\frac{h}{p}} \quad (3)$$

where p is the distance between the centers of two adjacent conductors. In (2) and (3), δ_w is the skin depth of the wire expressed as

$$\delta_w = \sqrt{\frac{\rho_w}{\pi \mu_o \mu_{rw} f}}. \quad (4)$$

In (4), ρ_w is the wire electric resistivity, μ_{rw} is the wire relative magnetic permeability (ρ_w = 17.24x10^{-9}Ωm and μ_{rw} = 1 for a copper conductor at 20°C), and μ_o= 4π 10^{-7} H/m.

The leakage inductance L_{ac}^l, related to the magnetic energy stored in the winding, is derived by Dowell [1]

$$L_{ac}^l = R_{wdc} \frac{A}{2\pi f} \cdot \left[\frac{e^{2A} - e^{-2A} - 2\sin(2A)}{e^{2A} + e^{-2A} - 2\cos(2A)} + 2\frac{N_l^2 - 1}{3} \cdot \frac{e^{A} - e^{-A} + 2\sin A}{e^{A} + e^{-A} + 2\cos A} \right]. \quad (5)$$

B. Core Model

The electrical parameters of the core are obtained through an one-dimensional analysis of the electromagnetic diffusion in a packet of laminations for sinusoidal steady state. Details on this study can be found in [2]. A similar study has been developed by the authors for ferrite-core inductors [4]. In the case of non-saturated laminated iron-core inductors, the expressions for the main inductance L_{ac}^m, related to the magnetic field paths in the core, and for the core equivalent series resistance R_c, related to the losses due to eddy currents flowing in the core, are [2]

$$L_{ac}^m = L_{dc}^m \frac{\delta_c}{s} \frac{\sinh\frac{s}{\delta_c} + \sin\frac{s}{\delta_c}}{\cosh\frac{s}{\delta_c} + \cos\frac{s}{\delta_c}} \quad (6)$$

and

$$R_c = 2\pi f L_{dc}^m \frac{\delta_c}{s} \frac{\sinh\frac{s}{\delta_c} - \sin\frac{s}{\delta_c}}{\cosh\frac{s}{\delta_c} + \cos\frac{s}{\delta_c}} \quad (7)$$

where L_{dc}^m is the value of the main inductance at low frequencies, s is the thickness of the lamination, and δ_c is the skin depth for the iron sheets given by

$$\delta_c = \sqrt{\frac{\rho_c}{\pi \mu_c f}}. \quad (8)$$

In (8), ρ_c and μ_c are the electric resistivity and the magnetic permeability of the iron sheets, respectively. The core hysteresis loss is neglected in this work.

Most of the inductors used in power electronics applications are realized with air gaps. In fact, the presence of an air gap is the most common way to linearize the behavior of the inductor over a large excursion range of the winding current, avoiding the core saturation and reducing the harmonic distortion. Let us consider a laminated core with an air gap. Fig. 2(a) displays one of the sheets of the packet which realizes the core, and Fig. 2(b) shows a linear development of this sheet along its geometrical axis. Assuming the magnetic field vector $\boldsymbol{H}_c$ in the sheet directed along the z-axis and dependent only on the coordinate x and time t, the Ampère's circuital law applied to a generic path, as the one indicated in Fig. 2(b), gives the following relationship

$$H_c(x,t)\, l_c + H_a(x,t)\, l_a = N\, i(t) + \int_x^{s/2} J_y(x,t)\, l_c\, dx \quad (9)$$

where H_a is the magnetic field in the air gap, $i(t)$ is the current flowing in the N turns of the coil, $J_y(x, t)$ is the density of the eddy currents in the sheet, l_c is the axial length of the iron sheet, and l_a is the length of the air gap. In the Appendix, it is shown that the expressions (6) and (7) are also valid for a non-saturated laminated iron-core inductor with an air gap if the equivalent permeability of the magnetic circuit

$$\mu_e = \mu_c \frac{l_c}{l_c + \mu_{rc}\, l_a} \quad (10)$$

is introduced in (8) instead of the iron magnetic permeability μ_c. In (10), μ_{rc} is the relative magnetic permeability of the iron.

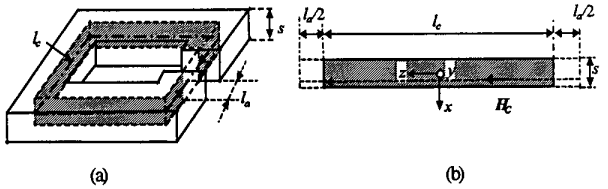

(a) (b)

Fig. 2. (a) Sheet of a packet.
(b) Linear development of a sheet along its axis.

C. Equivalent Circuit of Laminated Iron-Core Inductors

Fig. 1(a) shows a lumped parameter model of a laminated iron-core inductor, where $L_{ac} = L_{ac}^{m} + L_{ac}^{l}$ is the total inductance, $R_{ac} = R_w + R_c$ is the total ac resistance, and C is the overall parasitic capacitance [3]. In general, L_{ac}^{m}, L_{ac}^{l}, R_w and R_c are dependent on frequency f. Fig. 1(b) depicts a series equivalent circuit of the inductor where the equivalent series parameters L_s and R_s are [4]

$$L_s(\omega) = \frac{X_s(\omega)}{\omega} = \frac{L_{ac}(1-\omega^2 L_{ac}C - \frac{CR_{ac}^2}{L_{ac}})}{(1-\omega^2 L_{ac}C)^2 + (\omega C R_{ac})^2} \quad (11)$$

and

$$R_s(\omega) = \frac{R_{ac}}{(1-\omega^2 L_{ac}C)^2 + (\omega C R_{ac})^2} \quad (12)$$

with $\omega = 2\pi f$. The self-resonant frequency $f_r = \omega_r / (2\pi)$ of an inductor is defined as the frequency at which the reactance X_S is zero. Hence, from the expression (11) the total parasitic capacitance can be calculated as

$$C = \frac{1}{(\omega_r)^2 L_{ac}(\omega_r) + \frac{R_{ac}^2(\omega_r)}{L_{ac}(\omega_r)}}. \quad (13)$$

The value of total capacitance C is obtained from (13) using the measured self-resonant frequency, and it is assumed to be a constant parameter in the whole range of inductor operating frequencies. The value of C was also verified making measurements above the self-resonance, at which the capacitive branch becomes dominant with respect to the RL branch of Fig. 1(a).

III. EXPERIMENTAL RESULTS

Measurements were carried out to test the validity of the proposed model for three laminated iron-core inductors with air gaps. An HP 4192A LF Impedance Analyzer (5Hz-13MHz) equipped with an HP 16047A test fixture [5] was employed to achieve a higher accuracy, minimizing residual parameters and contact resistances. The tested inductors were arranged by the same EI core depicted in Fig. 3, in order to emphasize the winding contribution.

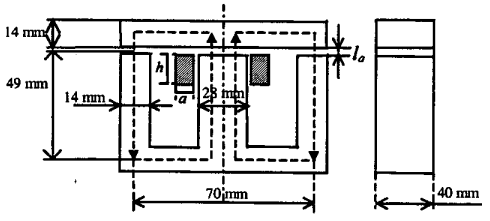

Fig. 3. Core view with a strip wire coil.

The value of the equivalent permeability of the EI core was calculated as

$$\mu_e = \mu_c \frac{l_c}{l_c + 2\mu_{rc} l_a} \quad (14)$$

where l_c is the length of the path consisting of the geometrical axis of the half central limb and that of one of two outer limbs, and $2l_a$ is the total air gap. The parameters of interest for the three types of inductors are reported in Table I. The low-frequency main inductance is calculated as $L_{dc}^{m} = \mu_e (N_l N_t)^2 l_c / A_{Fe}$, where N_l is the number of layers, N_t is the number of turns per layer, and A_{Fe} is the effective cross section area of the central limb. The magnetic permeability of the laminated iron-core used in the calculations corresponds to its initial value. The measured relative initial permeability was $\mu_{rci} = 300$. The measured electric resistivity of the iron sheet was $\rho_c = 7 \times 10^{-7}$ Ωm. The lamination thickness is $s = 0.3$ mm. Figs. 4 and 5 show the measured (dotted line) and calculated (solid line) equivalent series resistance R_S and reactance X_S of the tested inductor #1 as a function of frequency.

TABLE I
INDUCTOR PARAMETERS

	Inductor #1	Inductor #2	Inductor #3
Dimensions of the winding conductor (mm)	⊘ d=1.5	▨ h=5 a=2	⊘ d=1.46
p	$p \approx d$	$p \approx h$	$p \approx d$
N_l	6	3	2
N_t	23	6	24
A_{Fe} (mm²)	1067.36		
l_c (mm)	168		
l_a (mm)	0.4	0.5	0.21
μ_e/μ_o	123.53	107.69	175
L_{dc}^{m} (mH)	18.8	0.28	3.15
R_{wdc} (mΩ)	236	7	73
f_r (MHz)	0.103	3.051	1.485
C (pF)	152.95	62.32	20.69

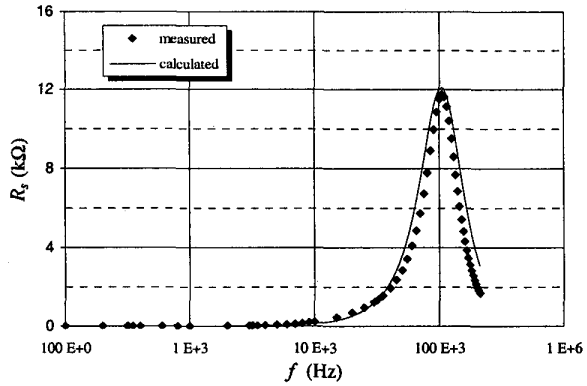

Fig. 4. Measured and calculated equivalent series resistance, R_S, for the inductor #1.

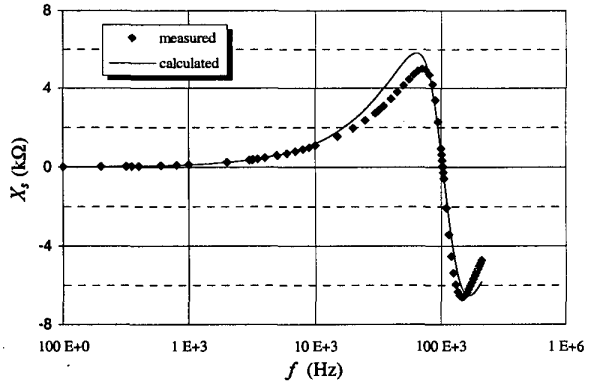

Fig. 5. Measured and calculated equivalent series reactance, X_S, for the inductor #1.

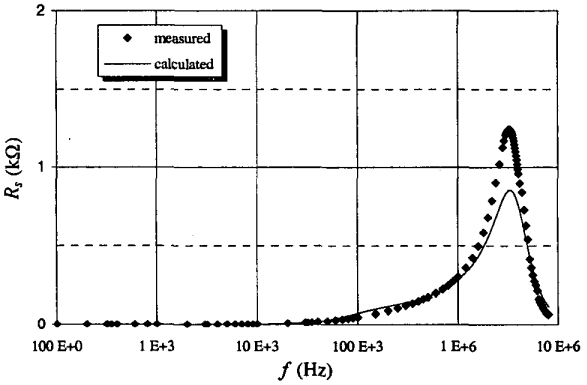

Fig. 6. Measured and calculated equivalent series resistance, R_S, for the inductor #2.

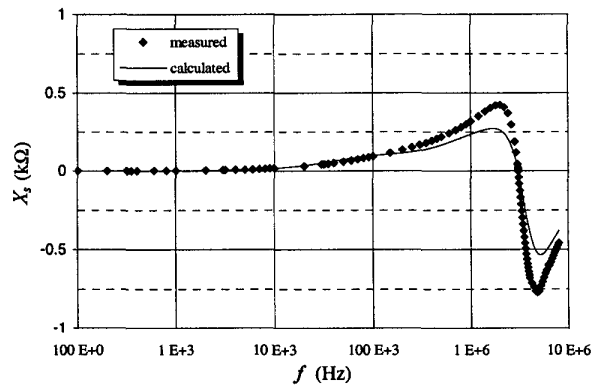

Fig. 7. Measured and calculated equivalent series reactance, X_S, for the inductor #2.

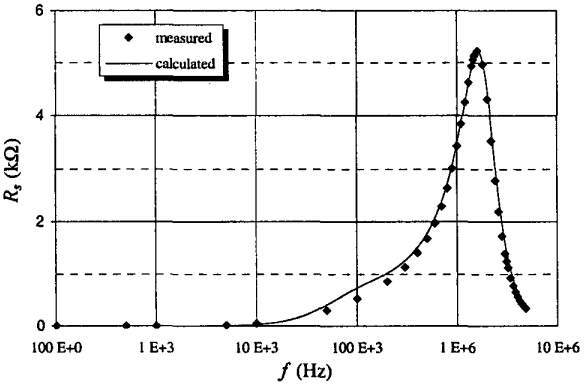

Fig. 8. Measured and calculated equivalent series resistance, R_S, for the inductor #3.

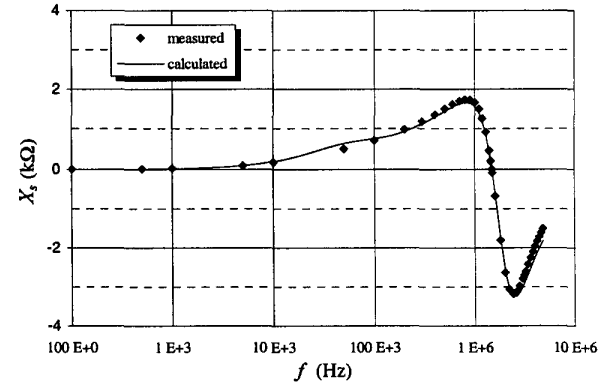

Fig. 9. Measured and calculated equivalent series reactance, X_S, for the inductor #3.

The measured (dotted line) and calculated (solid line) equivalent series resistance R_S and reactance X_S of the tested inductor #2 are depicted in Figs. 6 and 7, respectively.

The measured (dotted line) and calculated (solid line) equivalent series resistance R_S and reactance X_S of the tested inductor #3 are shown in Figs. 8 and 9, respectively.

The measured self-resonant frequency for the inductor #1 was f_r = 103.08 kHz. The capacitance value calculated through (13) was C = 152.95 pF. In the case of the inductor #2, the resonant frequency was f_r = 3.051 MHz, resulting in a calculated value of capacitance C = 62.32 pF. The inductor #3 presented its self-resonance at the measured frequency of f_r = 1.485 MHz and the calculated capacitance value was C = 20.69 pF. The calculated capacitance value for the inductor #1, arranged with six layers, is greater than the one of the inductor #3 with two layers. With reference to the inductors #1 and #3, the calculated capacitance values point out that the overall stray capacitance is smaller if the inductor is arranged by a low number of layers [6]. Besides, also the proximity effect in the winding resistance (1) and leakage inductance (5) is smaller if the number of layers is lower. The figures reported above show that the results obtained are in good agreement with the measurements also above the self-resonance.

The behavior of the total inductance L_{ac} versus frequency deserves to be investigated. Fig. 10 depicts the total inductance L_{ac}, the measured and calculated L_s for the inductor #1. This figure points out that the capacitance strongly affects the behavior of the inductor starting from about 80 kHz.

The total inductance L_{ac}, the measured and calculated L_s for the inductor #2 are shown in Fig. 11. The calculated curves L_{ac} and L_s coincide up to 3 MHz and above that frequency they move away from each other. It means that the effect of the overall stray capacitance is negligible up to 3 MHz and the decrease of the equivalent series inductance L_s is mainly due to the eddy currents. Above that frequency, the equivalent series inductance L_s quickly decreases crossing the zero-axis (parallel resonance) and assuming negative values which means that the presence of the overall stray capacitance C becomes dominant. The total inductance L_{ac}, the measured and calculated L_s for the inductor #3 are shown in Fig. 12. The parameters L_{ac} and L_s of the inductor #3 follow the same behavior described for the inductor #2 replacing the frequency of 3MHz with 1 MHz. The examined inductors underline that the effects due to the eddy currents in the laminated iron-core and the ones due to the stray turn-to-turn and turn-to-iron capacitances are important in different frequency ranges. Below the self-resonant frequency, the decrease of the main inductance L_{ac}^{m}, with respect to its low-frequency value, is mainly caused by the eddy currents in the laminated iron-core, as the magnetic field is expelled from the lamination by the eddy currents. For frequencies above the self-resonant frequency, the effect of the overall stray capacitance C becomes stronger than the eddy current effect.

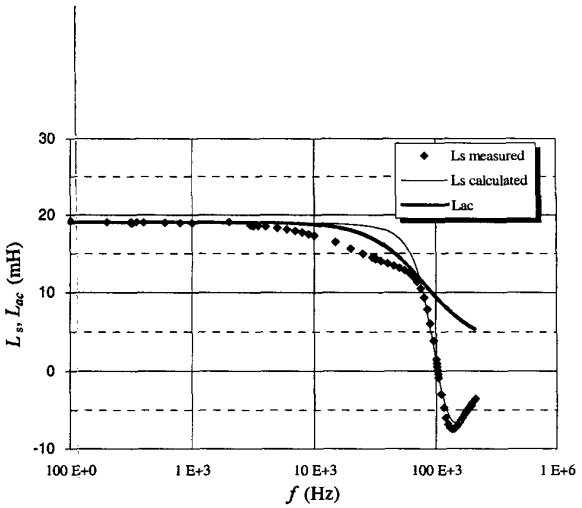

Fig. 10. Measured and calculated equivalent series inductance, L_S, and total inductance, L_{ac}, for the inductor #1.

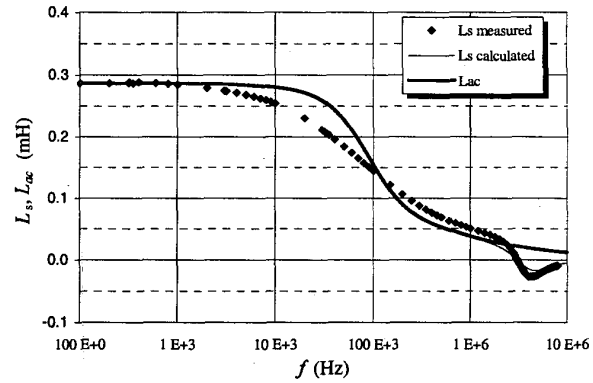

Fig. 11. Measured and calculated equivalent series inductance, L_S, and total inductance, L_{ac}, for the inductor #2.

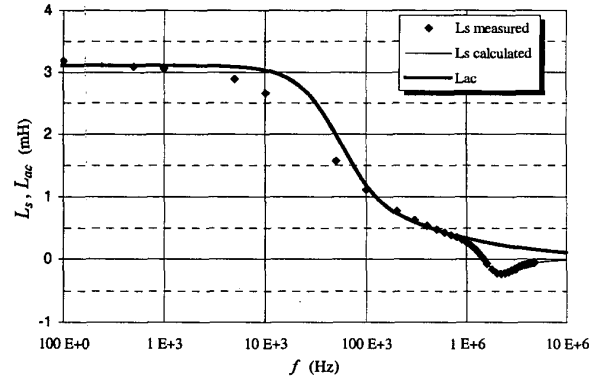

Fig. 12. Measured and calculated equivalent series inductance, L_S, and total inductance, L_{ac}, for the inductor #3.

IV. CONCLUSIONS

In this paper a *RLC* model is proposed to represent the behavior of laminated iron-core inductors for frequencies above the kHz range. The total ac resistance and total inductance are frequency-dependent parameters as they take into account skin and proximity effects in the winding and eddy currents in the laminated iron-core. The eddy currents are evaluated by an one-dimensional field analysis extended to cores with air gaps. The overall stray capacitance which models the turn-to-turn and turn-to-iron stray capacitances is calculated on the basis of the self-resonant frequency of the coil and it is assumed to be independent of frequency. The calculated results are in good agreement with the measurements carried out on three tested inductors. The presented model seems sufficiently accurate above the self-resonant frequency. It can be used for aided computer simulations of laminated iron-core inductors that are employed in switching converters.

APPENDIX

Let us consider a coil uniformly wound around a laminated iron-core of length *l*. The edge effects can be neglected assuming that the length of the packet of laminations is much larger than its cross sectional dimensions depicted in Fig. 13. The study is developed through an one-dimensional analysis of the electromagnetic diffusion in a packet of laminations in sinusoidal steady state [2].

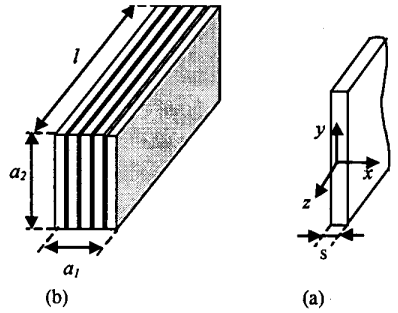

Fig. 13. (a) Packet of laminations and its dimensions. (b) Sheet and its thickness.

The time-varying magnetic field vector $\boldsymbol{H}$ is directed along the *z*-axis and dependent only on the *x* coordinate

$$\boldsymbol{H}(x,y,z,t) = H_z(x,t)\boldsymbol{a}_z . \tag{A1}$$

Introducing the magnetic field complex vector

$$\hat{\boldsymbol{H}}(x) = \hat{H}_z(x)\boldsymbol{a}_z \tag{A2}$$

the differential equation for the magnetic field in terms of the phasor $\hat{H}(x) = \hat{H}_z(x)$ is

$$\frac{d^2\hat{H}(x)}{dx^2} = \hat{k}^2\hat{H}(x) \tag{A3}$$

with

$$\hat{k}^2 = j\omega\mu_c/\rho_c . \tag{A4}$$

Equations (6) and (7) are obtained in [2] for a closed core by solving (A3) with appropriate boundary values.

Starting from (9), it will be shown that (6) and (7) are also valid in the case of laminated iron-cores with an air gap. Neglecting fringing effects in the air gap and taking into account the continuity of the magnetic flux density at the boundary between air and iron, it follows that

$$B_a(x,t) = B_c(x,t) . \tag{A5}$$

Substituting (A5) into (9) and considering linear constitutive laws in both the media, we obtain

$$H_c(x,t)l_c = \frac{\mu_e}{\mu_c}N\left[i(t)+\frac{1}{N}\int_x^{s/2} J_y(x,t)\,l_c\,dx\right] \tag{A6}$$

where μ_e is given by (10). From (A6), we can write

$$\frac{\partial H_c(x,t)}{\partial x} = \frac{\mu_e}{\mu_c}\frac{\partial}{\partial x}\left[\int_x^{s/2} J_y(x,t)dx\right]$$

$$= -\frac{\mu_e}{\mu_c}J_y(x,t). \tag{A7}$$

The Faraday's law for the problem under consideration can be written

$$\frac{\partial E_y(x,t)}{\partial x} = -\frac{\partial B_c(x,t)}{\partial t} . \tag{A8}$$

Taking Ohm's law $J_y = E_y/\rho_c$ into account and using (A7) and (A8) we can write

$$\frac{\partial^2 H_c(x,t)}{\partial x^2} = \frac{\mu_e}{\rho_c}\frac{\partial H_c(x,t)}{\partial t} . \tag{A9}$$

Introducing the magnetic field phasor $\hat{H}_c(x)$ in sinusoidal steady state, (A9) becomes

$$\frac{d^2\hat{H}_c(x)}{dx^2} = \hat{k}_t^2\hat{H}_c(x) \tag{A10}$$

where

$$\hat{k}_t^2 = j\omega\mu_e/\rho_c . \tag{A11}$$

The differential equation (A10) is identical to (A3). It leads to the same solutions given by (6) and (7), found in the case of a closed laminated iron-core, but the equivalent permeability (10) needs to be considered, resulting in a larger skin depth of the sheet. Hence, a laminated iron-core with air gaps is equivalent to a closed one when the equivalent permeability of the magnetic circuit is introduced.

REFERENCES

[1] P.J. Dowell, "Effects of eddy currents in transformer windings," *Proc. Inst. Elect. Eng.*, Vol. 113, pp. 1387-1394, Aug. 1966.

[2] J. Lammeraner and M. Stafl, *Eddy Currents*, London: Iliffe Books Ltd., 1966.

[3] G. Grandi, A. Massarini, M.K. Kazimierczuk, and U. Reggiani, "Stray capacitances of single-layer solenoid air-core inductors", *IEEE Trans. on Industry Applications*, Vol. 35, pp. 1162-1168, Sept. 1999.

[4] M.K. Kazimierczuk, G. Sancineto, G. Grandi, U. Reggiani, and A. Massarini, "High-frequency small-signal model of ferrite core inductors," *IEEE Trans. on Magnetics*, Vol. 35, pp. 4185-4191, Sept. 1999.

[5] *The Impedance Measurement Handbook.* Hewlett-Packard Co., 1989.

[6] A. Massarini and M. K. Kazimierczuk, " Self-capacitance of inductors," *IEEE Trans. on Power Electronics*, Vol. 12, pp. 671-676, July 1997.